optica

VECSEL systems for the generation and manipulation of trapped magnesium ions

S. C. Burd,[1,*] D. T. C. Allcock,[1] T. Leinonen,[2] J. P. Penttinen,[2] D. H. Slichter,[1] R. Srinivas,[1] A. C. Wilson,[1] R. Jördens,[1] M. Guina,[2] D. Leibfried,[1] and D. J. Wineland[1]

[1]Time and Frequency Division, National Institute of Standards and Technology, 325 Broadway, Boulder, Colorado 80305, USA
[2]Optoelectronics Research Centre, Tampere University of Technology, PO Box 692, FIN-33101 Tampere, Finland
*Corresponding author: shaun.burd@nist.gov

Received 10 June 2016; revised 11 September 2016; accepted 4 October 2016 (Doc. ID 268119); published 8 November 2016

Experiments in atomic, molecular, and optical (AMO) physics rely on lasers at many different wavelengths and with varying requirements on the spectral linewidth, power, and intensity stability. Vertical external-cavity surface-emitting lasers (VECSELs), when combined with nonlinear frequency conversion, can potentially replace many of the laser systems currently in use. Here, we present and characterize VECSEL systems that can perform all laser-based tasks for quantum information processing experiments with trapped magnesium ions. For the photoionization of neutral magnesium, 570.6 nm light is generated with an intracavity frequency-doubled VECSEL containing a lithium triborate crystal. External frequency doubling produces 285.3 nm light for a resonant interaction with the $^1S_0 \leftrightarrow {}^1P_1$ transition of neutral Mg. Using an externally frequency-quadrupled VECSEL, we implement Doppler cooling of $^{25}Mg^+$ on the 279.6 nm $^2S_{1/2} \leftrightarrow {}^2P_{3/2}$ cycling transition, repumping on the 280.4 nm $^2S_{1/2} \leftrightarrow {}^2P_{1/2}$ transition, coherent state manipulation, and resolved sideband cooling close to the motional ground state. Our systems serve as prototypes for applications in AMO requiring single-frequency, power-scalable laser sources at multiple wavelengths.

OCIS codes: (140.5960) Semiconductor lasers; (140.3515) Lasers, frequency doubled; (020.3320) Laser cooling; (270.5585) Quantum information and processing; (300.6320) Spectroscopy, high-resolution; (300.6520) Spectroscopy, trapped ion.

http://dx.doi.org/10.1364/OPTICA.3.001294

1. INTRODUCTION

Trapped ions provide a versatile experimental platform for research in quantum information processing [1–4], quantum simulation [5–8], and precision metrology [9,10]. Singly ionized magnesium has several desirable properties for ion trapping experiments. It has a cycling transition, which implies that only a single laser is required for Doppler cooling. High motional frequencies can be achieved with relatively low trap drive voltage due to the low atomic mass. The isotope $^{25}Mg^+$, with nuclear spin $I = 5/2$, has a series of intermediate magnetic field hyperfine "clock" qubits that are, to the first order, insensitive to magnetic field fluctuations. The ~1.7 GHz hyperfine splitting of these qubits facilitates manipulation with readily available commercial microwave electronics [11]. Magnesium ions have been used in experiments such as one of the earliest demonstrations of laser cooling [12] and microwave-driven two-qubit quantum logic gates [11]. However, generating the necessary high-power UV light presents a number of technical challenges.

For Mg^+ ion trapping applications, resonant two-photon ionization is generally used instead of direct excitation to the continuum at 7.646 eV, corresponding to 162.6 nm (all wavelengths listed in this work are vacuum wavelengths) [13]. As shown in Fig. 1(a), the photoionization (PI) laser, on resonance with the $3s^2\,{}^1S_0 \leftrightarrow 3s3p\,{}^1P_1$ transition of neutral magnesium at 285.3 nm, excites the atom. Photons from the PI laser or from another laser near 280 nm (for Doppler cooling Mg^+ ions) then have sufficient energy to ionize the excited atom. The energy levels employed for Doppler cooling, repumping, and quantum state manipulation are shown in Fig. 1(b). The $3s\,{}^2S_{1/2} \leftrightarrow 3p\,{}^2P_{3/2}$ transition provides a cycling transition for Doppler cooling and state detection. For quantum information experiments with $^{25}Mg^+$, pairs of appropriate Zeeman sublevels in the $3s\,{}^2S_{1/2}|F = 3\rangle$ and $|F = 2\rangle$ manifolds can serve as qubits. Coherent qubit manipulation can be achieved with stimulated Raman transitions, where the frequency difference between two Raman laser beams is set close to the qubit frequency [Fig. 1(b)]. Stimulated Raman transitions allow the coupling of internal degrees of freedom of the ions with their motional degrees of freedom [1], which is essential for implementing quantum logic gates and sub-Doppler cooling. Resolved sideband cooling can be used to cool trapped ions close to the motional ground state [1]. Preparation of a quantum system in a specific motional state with high probability is required for many quantum information experiments and for trapped-ion atomic clocks [9]. During resolved sideband cooling, it is necessary to repump the ion back to the initial hyperfine state.

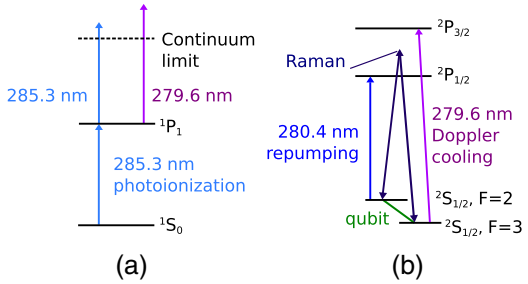

Fig. 1. Energy levels of (a) neutral magnesium relevant for photoionization and (b) $^{25}Mg^+$ relevant for Doppler cooling, repumping, and stimulated Raman transitions.

This can be accomplished efficiently using a laser resonant with the 3s $^2S_{1/2}\leftrightarrow$3p $^2P_{1/2}$ transition [14].

Magnesium ion trapping experiments have been performed traditionally with frequency-doubled traveling-wave dye lasers. More recently, frequency-quadrupled ytterbium fiber lasers [15,16] have been used to generate the light for Doppler cooling and qubit manipulation. However, these fiber lasers operate near the long wavelength edge of the amplification curve; thus, they are typically limited to about 2 W in the infrared (IR) at 1118 nm. To the best of our knowledge, commercial fiber laser systems are not currently available that can reach either 1120 nm for repumping on the $^2S_{1/2}\leftrightarrow{}^2P_{1/2}$ transition or 1141 nm for photoionization. Frequency-quadrupled diode laser systems are available that cover all required wavelengths for magnesium ion experiments [17]. These systems are currently limited to about 2 W of IR power if a tapered amplifier is used to amplify the diode seed laser. To achieve higher powers, amplification of a single-frequency seed laser can be accomplished with a Raman fiber amplifier [18]. High-power, widely tunable optical parametric oscillator (OPO) systems are also available but require a single-frequency pump source.

Here, we demonstrate laser systems for magnesium ion trapping experiments based on vertical external-cavity surface-emitting laser (VECSEL) technology. VECSELs exhibit many desirable properties for applications in high-precision spectroscopy [19]. The gain material can be designed for emission over a broad range of wavelengths, with demonstrations at 390 nm in the ultraviolet and at multiple wavelengths from 674 nm in the visible to 5 μm in the infrared [20]. The VECSEL geometry allows single-frequency emission with close to diffraction-limited output beam quality and a tuning range of tens of nanometers. External or intracavity harmonic generation extends the attainable wavelength range further into the visible and ultraviolet. The VECSEL architecture is intrinsically amenable to power scaling [20]. Single-frequency VECSELs with output powers of up to 23.6 W in the near IR have been reported [21]. Recently, a 0.56 W, 229 nm source from the fourth harmonic of a 916 nm VECSEL has been developed [22]. VECSEL systems with external harmonic generation have been used to perform Doppler-free spectroscopy of neutral mercury [23] and neutral rubidium [24].

Our systems consist of two laser designs, shown in Fig. 2. The first is an externally frequency-quadrupled VECSEL capable of generating 3.0 ± 0.1 W output power at 1117 nm that can be wavelength tuned for either laser cooling, repumping, or stimulated Raman transitions of Mg^+ ions. The second system, used for photoionization, is an intracavity frequency-doubled

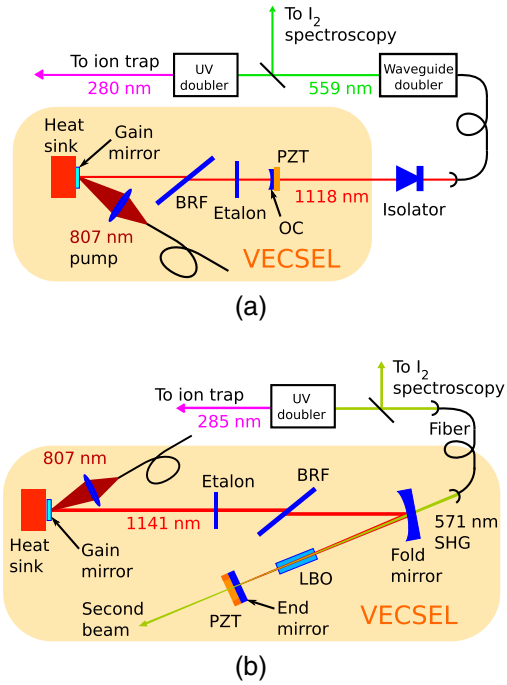

Fig. 2. VECSEL systems. (a) Externally quadrupled, I-cavity VECSEL system (IC system) used for Doppler cooling, repumping, and performing stimulated Raman transitions. (b) V-cavity, intracavity frequency-doubled system (VC system) for photoionization. PZT, piezo transducer; OC, output coupler; BRF, birefringent filter; LBO, lithium triborate; SHG, second harmonic generation.

VECSEL emitting up to 2.4 ± 0.1 W (total power in two output beams) at 571 nm and externally doubled to 285 nm. Both systems use commercial multi-mode diode lasers as pump sources.

2. LASER SETUP AND CHARACTERIZATION

We first consider the externally frequency-quadrupled, I-cavity VECSEL (IC system) shown in Fig. 2(a). The gain mirror employs the flip-chip design (upside-down growth structure with removed substrate) and consists of GaInAs/GaAs quantum wells strain compensated by GaAsP layers [25]. The gain chip is mounted on a diamond heat spreader, which is soldered to a copper plate. A thermoelectric cooler (TEC) module is clamped between the gain chip plate and a water-cooled micro-channel cooler for thermal management and temperature control. The 125-mm-long resonator has an I geometry consisting of a gain mirror and a 2% output coupler with a 200 mm radius of curvature (ROC). The end mirror is glued to a ring piezo-electric transducer (PZT) for controlling the cavity length. The gain chip is pumped with a fiber-coupled 807 nm multimode laser diode. The $1/e^2$ intensity pump spot diameter on the gain chip is roughly 400 μm. A 3-mm-thick quartz birefringent filter (BRF) plate, inserted at Brewster's angle, and a 1-mm-thick yttrium aluminum garnet (YAG) etalon are placed in the cavity to ensure single mode operation and to allow for wavelength selection. The etalon is positioned in a temperature-controlled oven for frequency stability and wavelength tuning. The VECSEL is contained in an insulated enclosure for acoustic and thermal isolation. With this system design, we have achieved 3.0 ± 0.1 W of IR power at 1117 nm with 21 ± 1 W of 807 nm pump power

(slope efficiency of 19 ± 1%). Light from the laser propagates through an optical isolator to prevent back reflection and is coupled into a commercial fiber-coupled quasi-phase-matched lithium niobate waveguide frequency doubler. We operate the frequency doubler at second harmonic (SH) powers below 300 mW to avoid potential damage to the waveguide. We obtain an overall conversion of 1118 to 559 nm of 22 ± 2% (including fiber coupling losses). SH light is coupled into a build-up cavity containing a β-barium borate (BBO) crystal for frequency doubling to 280 nm. Details of the cavity design are given by Wilson *et al.* [26]. With 1160 ± 40 mW in the IR, resulting in 260 ± 10 mW SH power, we generate 23 ± 2 mW in the UV with a visible-to-UV conversion efficiency of 9 ± 1%.

The laser linewidth in the UV must be much narrower than the width of the relevant atomic transitions (typically tens of MHz) to be of use for precision spectroscopy or Doppler cooling. In addition, resonant frequency doublers for generating UV light will convert laser frequency noise into intensity noise, which will degrade the fidelity of quantum manipulations performed using stimulated Raman transitions [27]. Figure 3 shows the relative intensity noise (RIN) spectrum of the IC system when producing 13 ± 1 mW at 280 nm. The experiment was performed using a photodiode connected to a fast Fourier transform analyzer, following the basic procedure described by Obarski and Splett [28]. The RIN in Fig. 3 is below −75 dBc/Hz above 10 kHz.

The "three-cornered hat" technique [29] was used to measure the short-term frequency fluctuations of the IC VECSEL in the infrared. Beams from the VECSEL, a single-mode fiber laser, and an external-cavity diode laser were combined and directed onto a single photodiode. The lasers' frequencies were set sufficiently close together that time-domain measurements of the beat notes of each pair of lasers could be recorded. The frequency of each laser was stabilized on slow time scales by locking to Doppler-free iodine spectroscopic features (closed-loop bandwidth <2 Hz), using a variation of the spectroscopic method described by Snyder *et al.* [30]. The data were processed to give the frequency deviation of each laser at different averaging times, as shown in Fig. 4. The VECSEL exhibits a frequency deviation below 20 kHz over all averaging times. For laser cooling and repumping experiments, it was necessary to stabilize the laser frequency to reduce slow drifts (over minute time scales). This was achieved either by locking the VECSEL to Doppler-free spectroscopic features of molecular iodine or performing a frequency offset lock [31] to an iodine-locked fiber laser. For stimulated Raman transitions, the free-running VECSEL frequency was sufficiently stable and active frequency control was not required.

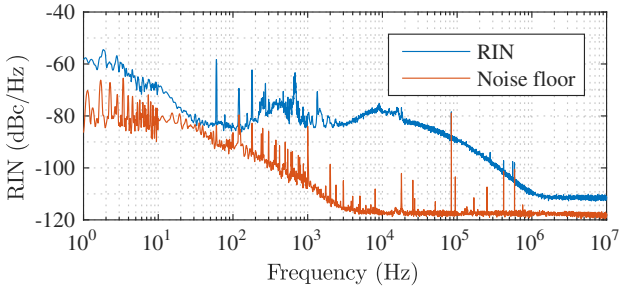

Fig. 3. 280 nm RIN spectrum. The noise floor is the spectrum obtained with the laser blocked and all other experimental parameters the same.

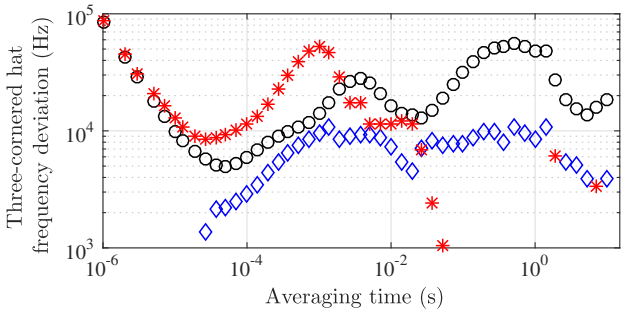

Fig. 4. Three-cornered hat frequency deviation (square root of the frequency variance) comparing the IC VECSEL system (blue diamonds) with a fiber laser (red stars) and an external-cavity diode laser (black circles).

We now consider the intracavity frequency-doubled VECSEL system for photoionization (VC system) as shown in Fig. 2(b). The same gain chip mechanical mount and thermal management are utilized as in the IC system. The flip-chip gain mirror consists of ten GaInAs quantum wells strain compensated by GaAsP. A more detailed description of the gain mirror design is given by Kantola *et al.* [32]. The fiber-coupled 807 nm multimode diode laser pump is focused onto the gain chip with a $1/e^2$ intensity diameter of roughly 380 μm. The cavity has a V geometry formed by the gain mirror, a fold mirror with a 100 mm ROC, and a plane end mirror. The mirrors are coated for high reflectivity from 1116 to 1142 nm and for high transmission at second harmonic wavelengths. A temperature-stabilized 3 × 3 × 15 mm lithium triborate (LBO) crystal, with dual anti-reflection coatings at 1141 and 571 nm and cut for type I phase matching, is placed in the 65 mm short arm of the cavity for second harmonic generation. A 1-mm-thick YAG etalon and a 3-mm-thick quartz BRF, inserted at Brewster's angle, are placed in the 125 mm long arm of the cavity for wavelength selection. A PZT is used for fine adjustment of the cavity length. Two separate 571 nm beams with roughly equal power exit the cavity through the fold and end mirrors. The laser can generate up to 1.2 ± 0.1 W in each output beam at 571 nm when the gain mirror is cooled to 8°C. The 571 nm light is frequency doubled to 285 nm using a build-up cavity with a BBO crystal. For the reduction of long-term frequency drifts, the VC laser can be locked to a Doppler-free molecular iodine transition. A scan over the Doppler-free iodine lines near 525.4050 THz is shown Fig. 5. From the locked error signal, we estimate a root mean squared (RMS) frequency deviation of 180 kHz over 6 min with a lock-in time constant of

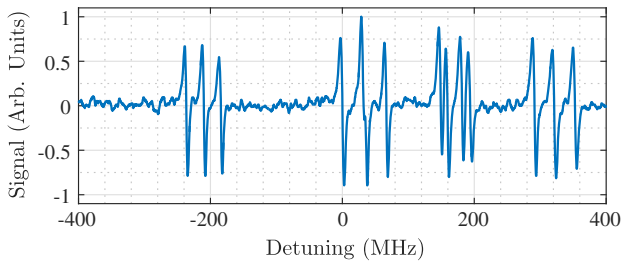

Fig. 5. Doppler-free scan of iodine lines relative to 525.4050 THz using the intracavity-doubled VC system.

10 ms. The short-term frequency fluctuations were measured by tuning the laser onto resonance with a reference cavity (finesse of 250 ± 10). From the electronic Hänsch–Couillaud error signal [33], we infer a laser linewidth of 50 ± 10 kHz using a detector bandwidth of 470 kHz.

3. ION TRAPPING AND SPECTROSCOPY

In our Mg ion trapping apparatus, a thermal beam of ^{25}Mg atoms is produced using an electrically heated oven containing isotopically enriched Mg. For photoionization, roughly 1 mW of laser light at 285 nm from the VC system is coupled into a solarization-resistant single-mode fiber [34] and focused to a calculated $1/e^2$ intensity diameter of 26 μm through the trapping region of a surface-electrode RF Paul trap similar to that used by Ospelkaus *et al.* [11]. Light at 280 nm for Doppler cooling is also applied to the trapping region. After allowing the oven to reach its steady-state operating temperature, we reliably and repeatably load single Mg^+ ions into the trap within 10 s.

For spectroscopy of the $^2S_{1/2} \leftrightarrow {}^2P_{3/2}$ transition, the IC system is frequency-offset locked to a fiber laser stabilized to a Doppler-free iodine line. UV light from the IC system is fiber coupled and focused onto the ion with a $1/e^2$ intensity diameter of approximately 24 μm. The frequency of the light is scanned by adjusting the drive frequency applied to an acousto-optic modulator (AOM). For each frequency point in the scan, photons scattered by the trapped ion were collected with a high-numerical-aperture objective and counted with a photomultiplier tube (PMT). The experiment was repeated 200 times for each frequency point. The UV light from the VECSEL was pulsed on for 25 μs during each experiment so as not to significantly change the motional state of the ion when the frequency is blue detuned (above the line center frequency). Figure 6 shows a scan of the laser frequency over the resonance. The atomic linewidth was measured to be 69 ± 3 MHz. The residual width above the natural linewidth of 41.8 MHz [35] is likely due to residual Doppler broadening. To demonstrate laser cooling, the laser was detuned by approximately 10 MHz below the line center frequency. The ion could be confined in the trap with no change in the ion lifetime compared to Doppler cooling with a fiber laser system.

Decoherence-assisted spectroscopy [35] was used to probe the $^2S_{1/2} \leftrightarrow {}^2P_{1/2}$ transition. Figure 6 shows the resulting spectrum. The IC system can be tuned over the ≃2.74 THz fine-structure splitting of $^{25}Mg^+$.

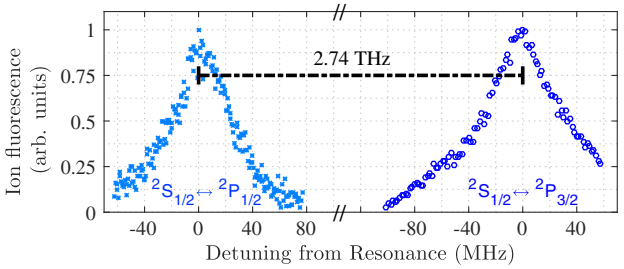

Fig. 6. Spectroscopy of the $^2S_{1/2} \leftrightarrow {}^2P_{1/2}$ and $^2S_{1/2} \leftrightarrow {}^2P_{3/2}$ transitions of a single trapped $^{25}Mg^+$ ion. The zero detuning points of the transitions from the $^2S_{1/2}$ to the $^2P_{1/2}$ and $^2P_{3/2}$ levels are relative to 1069.34 and 1072.08 THz, respectively [35]. The fine-structure separation is approximately 2.74 THz. Each spectrum is independently normalized.

For experiments involving stimulated Raman transitions, we choose a qubit consisting of the two hyperfine states $|\uparrow\rangle = {}^2S_{1/2}|F = 2, M_F = 2\rangle$ and $|\downarrow\rangle = {}^2S_{1/2}|F = 3, M_F = 3\rangle$. We use the IC system to perform resolved sideband cooling [1] of a Doppler-cooled trapped ion close to the quantum ground state of the trap. The frequency difference between the two Raman beams is set to the red sideband (RSB) frequency, the $|\downarrow\rangle \leftrightarrow |\uparrow\rangle$ transition frequency *minus* the frequency of the motional mode being cooled. An RSB pulse promotes transitions from $|\downarrow, n\rangle \leftrightarrow |\uparrow, n-1\rangle$, where n is the quantum number describing the motional state of the trapped ion [1]. Repumping then brings the qubit to the ground electronic state $|\downarrow, n-1\rangle$ with one less motional quantum. This sequence is repeated until the ion reaches the $|\downarrow, n = 0\rangle$ state. If the ion is close to the ground state, excitation of the ion at the red sideband frequency is strongly suppressed, whereas excitation of the $|\downarrow, n\rangle \leftrightarrow |\uparrow, n+1\rangle$ blue sideband (BSB) transition is not. Figure 7 shows frequency scans of the first red and blue sidebands for a radial motional mode of the trap after ground-state cooling using the IC system. Assuming that the occupations of the motional states have a thermal distribution after cooling, the average motional state occupation number $\langle n \rangle$ of a given motional mode can be calculated from the ratio of the heights of the RSB and BSB peaks for that mode [1]. From the data in Fig. 7, we calculate $\langle n \rangle = 0.008^{+0.013}_{-0.008}$, consistent with this radial mode being in the motional ground state with high probability. Rabi flopping on the $|\uparrow, n\rangle \leftrightarrow |\downarrow, n\rangle$ carrier transition of the qubit after ground-state cooling all three motional modes is shown in Fig. 8. For this experiment, we obtain a Rabi frequency of 191.1 ± 0.1 kHz and a $1/e$ decay time of 77 ± 3 μs. The decoherence is due to a combination of off-resonant photon scattering, magnetic field noise, and motional heating from nearby trap surfaces.

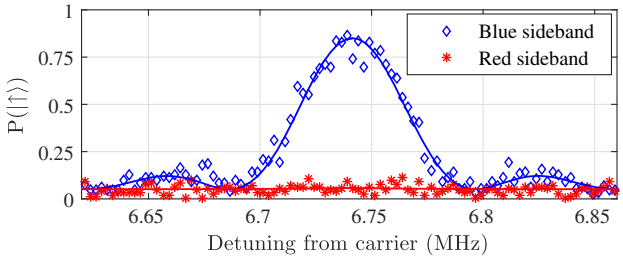

Fig. 7. The $|\uparrow\rangle$ state population of the first radial motional mode red and blue sidebands after ground-state cooling, from which we extract an average motional state occupation number $\langle n \rangle = 0.008^{+0.013}_{-0.008}$.

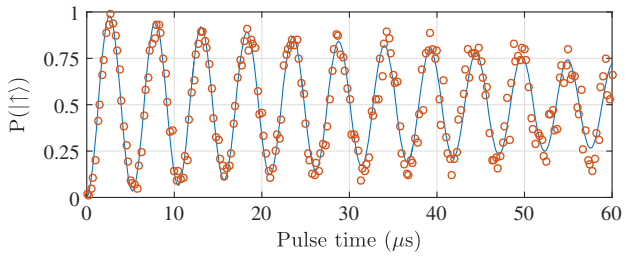

Fig. 8. Rabi flopping on the $|\downarrow\rangle \leftrightarrow |\uparrow\rangle$ carrier transition for a ground-state-cooled $^{25}Mg^+$ ion. The solid line is a exponentially decaying sinusoid, fitted to the data to give a Rabi frequency of 191.1 ± 0.1 kHz and a $1/e$ decay time of 77 ± 3 μs.

4. CONCLUSION

We have developed an optically pumped VECSEL system for generating the wavelengths required for producing, cooling, and manipulating magnesium ions. In the future, by the use of an 1118 nm → 559 nm frequency doubling stage with a higher optical damage threshold, our system should be capable of generating sufficient UV power for achieving fault-tolerant two-qubit entangling gates with stimulated Raman transitions [36]. This could be accomplished by intracavity frequency doubling, as in our VC laser setup, or through external resonantly enhanced second harmonic generation [16]. Typically, intracavity second harmonic generation has the advantage over external resonant frequency doubling that relatively high second harmonic powers can be generated in a simpler optical system. However, we have found that it is more difficult to reliably construct intracavity frequency-doubled VECSELs with the desired frequency stability and tunability for our applications. Our future work targets a better understanding of the challenges involved in using the two frequency-doubling schemes.

The power scalability of the VECSEL architecture makes it a promising candidate for systems that require individual laser addressing of multiple quantum systems. Due to their large wavelength tuning range, narrow linewidth, and low intensity noise, VECSEL systems have the potential to significantly reduce the complexity and cost of laser systems used for experiments in atomic and molecular physics.

Funding. NIST Quantum Information Program; Office of the Director of National Intelligence; Intelligence Advanced Research Projects Activity (IARPA); Office of Naval Research (ONR); Suomen Akatemia Project QUBIT (278388); Tekes (Finnish Funding Agency for Innovation) Project ReLase (40064/14).

Acknowledgment. We thank Dr. Jeff Sherman for assistance with the three-cornered hat data collection and analysis. We also thank Dr. David Hume and Dr. Yong Wan for their comments on the paper.

REFERENCES

1. D. Leibfried, R. Blatt, C. Monroe, and D. J. Wineland, "Quantum dynamics of single trapped ions," Rev. Mod. Phys. **75**, 281–324 (2003).
2. A. Steane, "The ion trap quantum information processor," Appl. Phys. B **64**, 623–643 (1997).
3. D. F. V. James, "Quantum dynamics of cold trapped ions with application to quantum computation," Appl. Phys. B **66**, 181–190 (1998).
4. R. Blatt and D. J. Wineland, "Entangled states of trapped atomic ions," Nature **453**, 1008–1015 (2008).
5. J. W. Britton, B. C. Sawyer, A. C. Keith, C. C. J. Wang, J. K. Freericks, H. Uys, M. J. Biercuk, and J. J. Bollinger, "Engineered two-dimensional Ising interactions in a trapped-ion quantum simulator with hundreds of spins," Nature **484**, 489–492 (2012).
6. R. Blatt and C. F. Roos, "Quantum simulations with trapped ions," Nat. Phys. **8**, 277–284 (2012).
7. C. Monroe, W. C. Campbell, E. E. Edwards, R. Islam, D. Kafri, S. Korenblit, A. Lee, P. Richerme, C. Senko, and J. Smith, "Quantum simulation of spin models with trapped ions," in *Proceedings of the International School of Physics 'Enrico Fermi,' Course 189*, M. Knoop, I. Marzoli, and G. Morigi, eds. (2015), pp. 169–187.
8. C. Schneider, D. Porras, and T. Schaetz, "Experimental quantum simulations of many-body physics with trapped ions," Rep. Prog. Phys. **75**, 024401 (2012).
9. T. Rosenband, D. B. Hume, P. O. Schmidt, C. W. Chou, A. Brusch, L. Lorini, W. H. Oskay, R. E. Drullinger, T. M. Fortier, J. E. Stalnaker, S. A. Diddams, W. C. Swann, N. R. Newbury, W. M. Itano, D. J. Wineland, and J. C. Bergquist, "Frequency ratio of Al^+ and Hg^+ single-ion optical clocks; metrology at the 17th decimal place," Science **319**, 1808–1812 (2008).
10. S. Kotler, N. Akerman, N. Navon, Y. Glickman, and R. Ozeri, "Measurement of the magnetic interaction between two bound electrons of two separate ions," Nature **510**, 376–380 (2014).
11. C. Ospelkaus, U. Warring, Y. Colombe, K. R. Brown, J. M. Amini, D. Leibfried, and D. J. Wineland, "Microwave quantum logic gates for trapped ions," Nature **476**, 181–184 (2011).
12. D. J. Wineland, R. E. Drullinger, and F. L. Walls, "Radiation-pressure cooling of bound resonant absorbers," Phys. Rev. Lett. **40**, 1639–1642 (1978).
13. D. N. Madsen, S. Balslev, M. Drewsen, N. Kjærgaard, Z. Videsen, and J. W. Thomsen, "Measurements on photo-ionization of $3s3p\,^1P_1$ magnesium atoms," J. Phys. B **33**, 4981–4988 (2000).
14. Y. Wan, F. Gebert, F. Wolf, and P. O. Schmidt, "Efficient sympathetic motional-ground-state cooling of a molecular ion," Phys. Rev. A **91**, 043425 (2015).
15. B. Hemmerling, F. Gebert, Y. Wan, D. Nigg, I. V. Sherstov, and P. O. Schmidt, "A single laser system for ground-state cooling of $^{25}Mg^+$," Appl. Phys. B **104**, 583–590 (2011).
16. A. Friedenauer, F. Markert, H. Schmitz, L. Petersen, S. Kahra, M. Herrmann, T. Udem, T. W. Hänsch, and T. Schätz, "High power all solid state laser system near 280 nm," Appl. Phys. B **84**, 371–373 (2006).
17. J. Zhang, W. H. Yuan, K. Deng, A. Deng, Z. T. Xu, C. B. Qin, Z. H. Lu, and J. Luo, "A long-term frequency stabilized deep ultraviolet laser for Mg^+ ions trapping experiments," Rev. Sci. Instrum. **84**, 123109 (2013).
18. Y. Feng, L. R. Taylor, and D. B. Calia, "150 W highly-efficient Raman fiber laser," Opt. Express **17**, 23678–23683 (2009).
19. S. C. Burd, D. Leibfried, A. C. Wilson, and D. J. Wineland, "Optically pumped semiconductor lasers for atomic and molecular physics," Proc. SPIE **9349**, 93490P (2015).
20. M. Kuznetsov, "VECSEL semiconductor lasers: A path to high-power, quality beam and UV to IR wavelength by design," in *Semiconductor Disk Lasers: Physics and Technology*, O. G. Okhotnikov, ed. (Wiley-VCH, 2010), Chap. 1.
21. F. Zhang, B. Heinen, M. Wichmann, C. Möller, B. Kunert, A. Rahimi-Iman, W. Stolz, and M. Koch, "A 23-watt single-frequency vertical-external-cavity surface-emitting laser," Opt. Express **22**, 12817–12822 (2014).
22. Y. Kaneda, J. M. Yarborough, Y. Merzlyak, A. Yamaguchi, K. Hayashida, N. Ohmae, and H. Katori, "Continuous-wave, single-frequency 229 nm laser source for laser cooling of cadmium atoms," Opt. Lett. **41**, 705–708 (2016).
23. J. Paul, Y. Kaneda, T.-L. Wang, C. Lytle, J. V. Moloney, and R. J. Jones, "Doppler-free spectroscopy of mercury at 253.7 nm using a high-power, frequency-quadrupled, optically pumped external-cavity semiconductor laser," Opt. Lett. **36**, 61–63 (2011).
24. B. Cocquelin, D. Holleville, G. Lucas-Leclin, I. Sagnes, A. Garnache, M. Myara, and P. Georges, "Tunable single-frequency operation of a diode-pumped vertical external-cavity laser at the cesium D_2 line," Appl. Phys. B **95**, 315–321 (2009).
25. S. Ranta, T. Hakkarainen, M. Tavast, J. Lindfors, T. Leinonen, and M. Guina, "Strain compensated 1120 nm GaInAs/GaAs vertical external-cavity surface-emitting laser grown by molecular beam epitaxy," J. Cryst. Growth **335**, 4–9 (2011).
26. A. C. Wilson, C. Ospelkaus, A. P. VanDevender, J. A. Mlynek, K. R. Brown, D. Leibfried, and D. J. Wineland, "A 750-mW, continuous-wave, solid-state laser source at 313 nm for cooling and manipulating trapped $^9Be^+$ ions," Appl. Phys. B **105**, 741–748 (2011).
27. D. J. Wineland, C. Monroe, W. M. Itano, D. Leibfried, B. E. King, and D. M. Meekhof, "Experimental issues in coherent quantum-state manipulation of trapped atomic ions," J. Res. Natl. Inst. Stand. Technol. **103**, 259–328 (1998).
28. G. E. Obarski and J. D. Splett, "Transfer standard for the spectral density of relative intensity noise of optical fiber sources near 1550 nm," J. Opt. Soc. Am. B **18**, 750–761 (2001).
29. J. E. Gray and D. W. Allan, "A method for estimating the frequency stability of a single oscillator," in *Proceedings of the 28th Annual Symposium on Frequency Control* (1974), pp. 243–246.
30. J. J. Snyder, R. K. Raj, D. Bloch, and M. Ducloy, "High-sensitivity nonlinear spectroscopy using a frequency-offset pump," Opt. Lett. **5**, 163–165 (1980).

31. A. Castrillo, E. Fasci, G. Galzerano, G. Casa, P. Laporta, and L. Gianfrani, "Offset-frequency locking of extended-cavity diode lasers for precision spectroscopy of water at 1.38 μm," Opt. Express **18**, 21851–21860 (2010).
32. E. Kantola, T. Leinonen, S. Ranta, M. Tavast, and M. Guina, "High-efficiency 20 W yellow VECSEL," Opt. Express **22**, 6372–6380 (2014).
33. T. W. Hänsch and B. Couillaud, "Laser frequency stabilization by polarization spectroscopy of a reflecting reference cavity," Opt. Commun. **35**, 441–444 (1980).
34. Y. Colombe, D. H. Slichter, A. C. Wilson, D. Leibfried, and D. J. Wineland, "Single-mode optical fiber for high-power, low-loss UV transmission," Opt. Express **22**, 19783–19793 (2014).
35. G. Clos, M. Enderlein, U. Warring, T. Schaetz, and D. Leibfried, "Decoherence-assisted spectroscopy of a single Mg^+ ion," Phys. Rev. Lett. **112**, 113003 (2014).
36. R. Ozeri, W. M. Itano, R. B. Blakestad, J. Britton, J. Chiaverini, J. D. Jost, C. Langer, D. Leibfried, R. Reichle, S. Seidelin, J. H. Wesenberg, and D. J. Wineland, "Errors in trapped-ion quantum gates due to spontaneous photon scattering," Phys. Rev. A **75**, 042329 (2007).